PHYSICAL REVIEW E **109**, 044701 (2024)

Anchoring-mediated stick-slip winding of cholesteric liquid crystals

Weichao Zheng [*]
Department of Chemistry, Physical and Theoretical Chemistry Laboratory, University of Oxford, Oxford OX1 3QZ, United Kingdom

(Received 11 May 2023; revised 15 November 2023; accepted 13 March 2024; published 9 April 2024)

The stick-slip phenomenon widely exists in contact mechanics, from the macroscale to the nanoscale. During cholesteric-nematic unwinding by external fields, there is controversy regarding the role of planar surface anchoring, which may induce discontinuous stick-slip behaviors despite the well-known continuous transitions observed in past experiments. Here we observe three regimes, namely, constrained, stick-slip, and sliding-slip, under mechanical winding with different anchoring conditions, and measure the corresponding forces by the surface force balance. These behaviors result from a balance of cholesteric elastic torque and surface torque, reminiscent of the slip morphology on frictional substrates [T. G. Sano *et al.*, Phys. Rev. Lett. **118**, 178001 (2017)], and provide evidence of dynamics in static rotational friction.

DOI: 10.1103/PhysRevE.109.044701

I. INTRODUCTION

In broad soft matter areas, including turbulence [1], micro- and nanofluidics [2], and yield stress materials [3], boundary conditions are important for material properties and performance. Similarly, in liquid crystals, surface anchoring also plays a crucial role in the order parameter, the temperature of the nematic-isotropic phase transition [4], and the response of molecules to external fields [5], especially in confined geometries such as liquid crystal displays. With strong anchoring, there exists a critical threshold voltage that orients the nematic molecules, called the Fréedericksz transition [6], below which molecules are still. However, there is a debate about whether planar anchoring affects the cholesteric-nematic unwinding transition by external fields.

Decades ago, it was predicted [5,7] and proven [8–11] that magnetic or electric fields can continuously unwind cholesterics to nematics, but the situation with different planar anchoring conditions was not explicitly addressed by experiments. Some studies [7,12,13] suggested that the continuous cholesteric-nematic transition is only applicable for bulk samples in which the surface anchoring is negligible. By varying the anchoring strength in confinement, rich behaviors, such as stick-slip or stepwise transitions, were predicted to happen under external stimuli [7,13–27], including temperature, light, stress, and magnetic and electric fields. In particular, a recent study [28] reported that if the easy axis on one surface rotates, chiral nematics may show three regimes, including free twist, stick-slip, and constrained winding, as a balance of twist elastic torque and surface torque [20,28–30]. Although some evidence of discontinuous transitions has been presented [12,31–37], different mechanisms were still discussed, probably due to the experimental precision and the complexity of surface anchoring, and none of the models could be directly applied to explain the observations in this work.

Here, we use surface force balance (SFB) to simultaneously measure the optical and mechanical responses of cholesterics along the helical axis under various boundary conditions. Desiccated cholesterics were confined between two freshly cleaved muscovite mica surfaces that were glued onto crossed cylinders. In the beginning, a strong planar anchoring was obtained, but anchoring strength decayed over time mainly due to the adsorption of water from the ambient environment [38,39]. Therefore, three different regimes were observed during experiments, resulting from the decayed frictional surface torque. Furthermore, the hysteresis of twist transitions was observed during the retraction and approach of surfaces in all three regimes.

II. RESULTS

A. Three regimes

Cholesteric layers with a layer thickness of half pitch $p = 122$ nm were compressed in the SFB [40] (Fig. 1(a) and Fig. S1 in the Supplemental Material [41]) with a cylinder radius of R. The thickness of a layer (or an integer layer) mentioned in the following text refers to a π rotation of molecules, i.e., half pitch p. With time evolution, three regimes of the measured force profiles were observed [Fig. 1(b)]. In the first regime, the force generated by the constrained cholesterics initially started from zero and increased with increasing strain to 65%, peaking at 14 mN/m before the surface jumped into the contact position, and all the cholesterics were squeezed out together. In the second regime, stick-slip jumps of the surface occurred after the force accumulated to 1.5 mN/m with about 30% strain, and finally, the surfaces jumped to contact. The number of jumps corresponded to five integer layers and a noninteger layer (less than a π rotation) since the easy axes on mica surfaces were not parallel [40]. Sometimes,

---

[*] zwhich@outlook.com

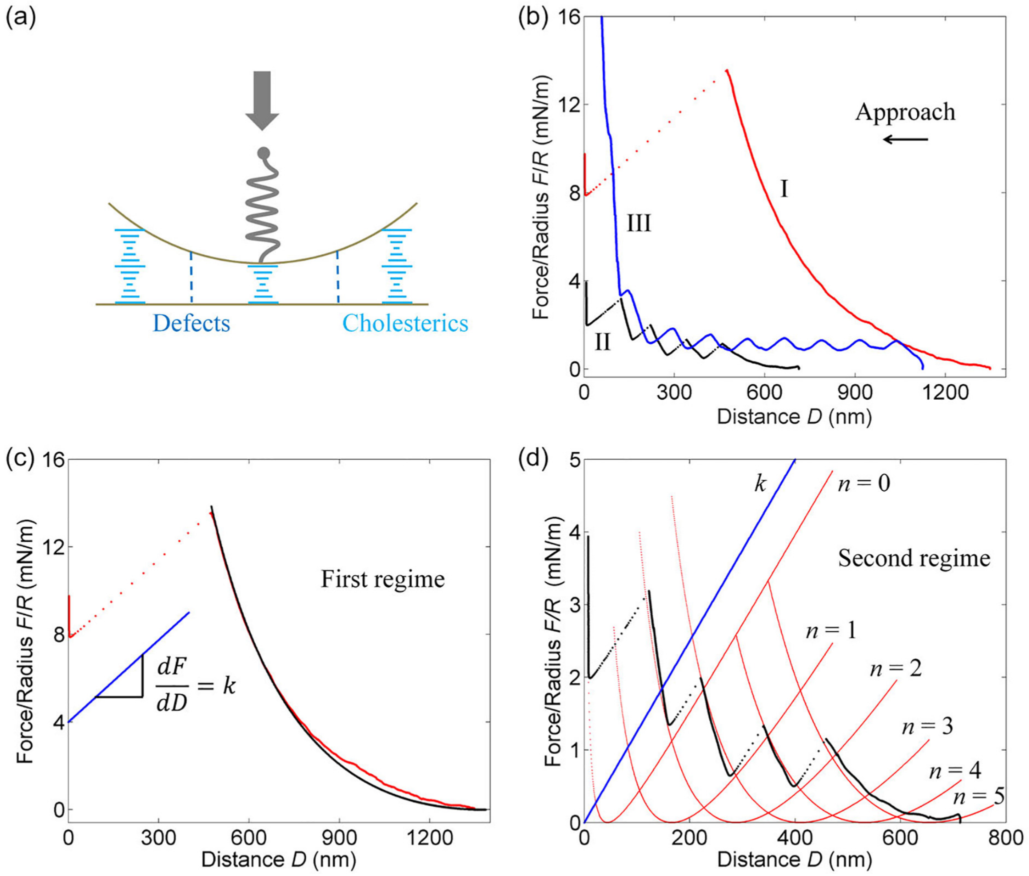

FIG. 1. Forces measured in the surface force balance (SFB). (a) Schematic diagram of cholesterics confined in the crossed cylinders with radius R. (b) Force profiles of three regimes, i.e., I: Constrained (red); II: Stick-slip (black): and III: Sliding-slip (blue), during the approach of the surface as the anchoring strength decreases. (c) Force profile (red, light gray) in the first regime fitted by elastic forces (black, dark gray) calculated by Eq. (4) with $K_{22} = 3.8$ pN. (d) Force profile (black, dark gray) in the second regime fitted by elastic forces (red, light gray) calculated by Eq. (4) with various integer layers (numbers) and $K_{22} = 6$ pN. The slope of the straight blue line in (c,d) is the spring constant of the cantilever spring that connects to the surface $dF/dD = k = 125$ N/m.

multiple-layered jumping events were observed in this regime (Fig. 1(b) and Fig. S2 [41]). In the last regime, the surface jumped periodically with a wavelength equal to the half pitch without a large deformation of cholesterics, and the last few layers were difficult to squeeze out (i.e., the final layers resisted the surface approach with larger forces compared to the previous layers, which will be discussed in Sec. III), resulting in large forces. It is worth noting that there was a constant background force of around 1 mN/m in this regime.

B. Free energy

In cholesterics, the free energy per unit area is formed by the elastic energy and the anchoring energy from both surfaces. The anchoring potential is not a well-defined term; thus, a general parabolic form is given below,

$$G = \int_0^D \frac{1}{2}K_{22}(\phi' - q_0)^2 dD + W\left(\frac{\Phi_0 - \Phi}{2}\right)^2, \tag{1}$$

where D is the closest surface separation between two crossed cylinders; K_{22} is the twist elastic constant; $\phi' = \frac{\partial \Phi}{\partial D} = \frac{\Phi}{D}$ is the molecular rotation rate at a distance D with a total twist angle Φ, which is constant for a uniform sample; W is the anchoring strength; Φ_0 is the original twist angle; and q_0 is the natural molecular rotation rate at relaxation. By ignoring the anchoring energy with a strong boundary, the free energy becomes

$$G = \frac{1}{2}K_{22}\left(\frac{\Phi}{D} - q_0\right)^2 D. \tag{2}$$

With a strong anchoring, the twist angle $\Phi \approx \Phi_0 = q_0 D_0^n$ keeps the original rotation rate at a starting distance D_0^n with n layers. Thus, the free energy G^n and the generated force F with Derjaguin approximation are written as

$$G^n = \frac{1}{2}K_{22}{q_0}^2 \frac{\left(D_0^n - D\right)^2}{D}, \tag{3}$$

$$F = 2\pi R G^n = \pi R K_{22}{q_0}^2 \frac{\left(D_0^n - D\right)^2}{D}. \tag{4}$$

Figure 1(c) shows that the match between the experiment and theory [Eq. (4)] is good, indicating that the anchoring strength in the first regime is strong. The slope of the jump-in is comparable to the spring constant, which manifests that the spring instability dominates the jumping process [40]. The elastic deformation almost without dissipation [42] works like an ideal spring, neglecting the effect of gravity at the micro- and nanoscale. This deformation, which can last for more than 1 h without dissipation if the surface stops moving (Fig. S3 [41]), is truly elastic rather than viscous.

In the second regime, the force profile can also be fitted by the harmonic elastic forces calculated using Eq. (4) with various layers of cholesterics [Fig. 1(d)]. The crossing points of the harmonic forces fall on distances equal to the integer number of quarter pitch (Fig. S4 [41]). Notably, the jumping distances are smaller than theoretical values, which could be due to the expansion of dislocation defects that store elastic energy. The effect of defects is discussed in Sec. SII of the Supplemental Material [41] (including Refs. [5,7,10,12–29,31–35,37,40,42,43–62]). In the first and second regimes, two values of K_{22} were used to fit the experimental data, which will be discussed in the next section.

III. DISCUSSION

A. Decayed anchoring strength

The compression ratio that cholesterics can sustain with time decreases from the first to the third regime, indicating a decrease in anchoring strength after the adsorption of water from the ambient environment [38,39]. In the third regime, surfaces are difficult to compress to contact, which supports the assumption that surfaces change with time. There are several possible reasons why a hard wall is encountered before contact. Firstly, the adsorbed water dissolves and accumulates potassium ions from mica surfaces to the contact position, which increases the electrostatic repulsion. Secondly, liquid crystal molecules grow epitaxially with time [63]. Thirdly, contaminants from the ambient air adsorb to the surface.

These three regimes emerge with the change of anchoring strength. Considering the longer timescale, more regimes might appear. For example, if the adsorbed water changes the direction of the easy axis on the mica surface [38,39], the behaviors could be different. Finally, if the mica surfaces become totally homeotropic, the pitch axis will be parallel with the surface, causing fingerprint textures and more isotropiclike optics.

B. Surface torque

The measured forces follow the twist elastic theory very well with manual input of the twist angle, but three different regimes varying with anchoring strength are obtained, namely, constrained, stick-slip, and sliding-slip. What is the mechanism that determines the critical threshold of the jump in different regimes?

When cholesterics are confined between two plates, the elastic torque is balanced by the surface torque, which includes the surface anchoring and surface viscosity [28–30]. For strong anchoring, molecules deviate very slowly from the easy axis; thus the torque from surface viscosity is negligible. However, at mediate anchoring, molecules slide to a deviated angle with a larger speed; therefore, both surface anchoring and surface viscosity balance with elastic torque. The torque balance can be written as

$$K_{22}\left(\frac{\partial \Phi}{\partial D} - q_0\right) = W\frac{\Phi_0 - \Phi}{2} - \gamma_s\frac{\partial \Phi}{\partial t}, \tag{5}$$

where W is the anchoring strength, γ_s is the surface viscosity, and t is the time.

With strong anchoring, the surface viscosity and anchoring deviation are neglected here. The elastic torque Γ_e is mainly balanced by the anchoring torque Γ_a,

$$\Gamma_e = K_{22}\left(\frac{\Phi}{D} - q_0\right) = \Gamma_a = W\frac{\Phi_0 - \Phi}{2}, \tag{6}$$

$$K_{22}q_0\left(\frac{D_0}{D} - 1\right) = W\frac{\Phi_0 - \Phi}{2}. \tag{7}$$

For a more rigorous calculation that considers anchoring deviations, the surface distance D in Eq. (6) is calculated as

$$D = \frac{K_{22}\Phi}{K_{22}q_0 + W\frac{\Phi_0 - \Phi}{2}}. \tag{8}$$

At the critical torque threshold Γ_c, the critical twist angle Φ_c and critical surface distance D_c are calculated below:

$$\Phi_c = \Phi_0 - \frac{2\Gamma_c}{W}, \tag{9}$$

$$D_c = \frac{K_{22}\left(\Phi_0 - \frac{2\Gamma_c}{W}\right)}{K_{22}q_0 + \Gamma_c} = \frac{D_0 - \frac{2\Gamma_c}{q_0 W}}{1 + \frac{\Gamma_c}{K_{22}q_0}}. \tag{10}$$

Figures 2(a) and 2(b) show that there exists a threshold constant of the compression ratio, about 35% and 75% in the first and second regimes, respectively, for the surface to sustain the elastic stress at a certain anchoring condition, no matter how many layers are compressed. This constant ratio manifests that there is a threshold anchoring torque Γ_c that is analogous to the breakaway friction torque [64], a concept from rotational friction. When the anchoring is strong, the frictional torque can sustain a large elastic torque, such that cholesteric layers will not jump until the threshold is reached.

The anchoring torque in the first and second regimes is plotted in Fig. 2(c), where the first regime and second regimes fall on two slopes of calculation based on Eq. (7) with twist elastic constant $K_{22} = 3.8$ and 6 pN, respectively. The twist elastic constant should be a consistent value across regimes. Here, however, we treat K_{22} as the only fitting parameter of Eqs. (4) and (7), taking all unknown factors into account. Then the fitting parameter K_{22} is compared with the reported value [47] of 6.18 pN. If the force profile in Fig. 1(c) is carefully examined, one can see that the slope at small compression is actually higher than the calculation with $K_{22} = 3.8$ pN and can be better fitted by 6 pN (Fig. S6(a) [41]). Therefore, the force profile in the first regime can be fitted by two values of K_{22}. The larger value is the material property [47], while the smaller one comes from unknown factors. This force deviation may be because mica surfaces on cylindrical lenses are not large enough, such that at small compression, the forces mainly generated near the contact position are free from the effect of mica areas, but at the large compression, mica areas start to limit the force responses, producing smaller forces. From the fitted elastic constant, we can estimate the effective coverage of mica on lenses is two-thirds.

C. Constrained regime

From Fig. 3(a), the slope and intersection obtained from the trend line are used to calculate the anchoring strength by

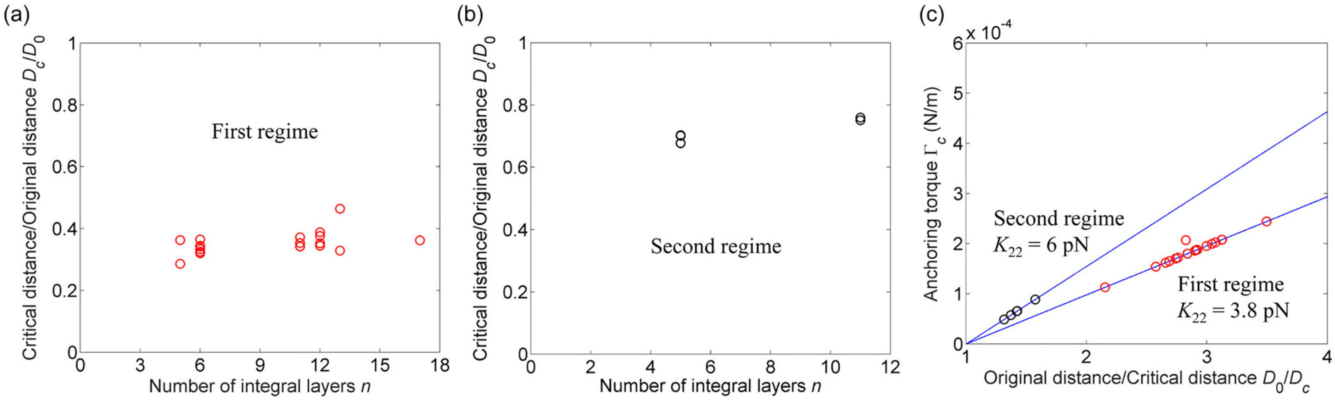

FIG. 2. Compression ratio of cholesteric layers at the critical jumping distance. (a) First regime. (b) Second regime (premier jumps). (c) The data in the first and second regimes fall on two blue lines that are theoretically calculated by Eq. (7) with $K_{22} = 3.8$ and 6 pN, respectively.

Eq. (10). Therefore, we obtain the critical anchoring torque $\Gamma_c \approx 0.23$ mN/m and anchoring strength $W \approx 0.15$ mN/m with $K_{22} = 6$ pN and half pitch $p = 122$ nm. The deviated angle on one surface can be calculated $\frac{\Phi_0 - \Phi}{2} \approx 0.49\pi$, where Φ_0 is the original twist angle and Φ is the instant twist angle, which means the molecules on each surface deviate around 90° from the easy axis at the jump threshold. Notably, no mathematical solution was found with the Rapini-Papoula potential [5], but the anchoring potential with other forms may also be feasible. For example, if the anchoring torque is $\frac{1}{2}W\frac{\Phi_0 - \Phi}{2}$ differentiated from the anchoring energy $\frac{1}{2}W(\frac{\Phi_0 - \Phi}{2})^2$, the anchoring strength will be 0.3 mN/m, but the critical torque and deviated angle are independent of the form of the anchoring potential. The exact anchoring potential could be further confirmed by optical observation of the deviated angle [65]. With the obtained anchoring strength and deviated angle, the measured forces in the first regime [Fig. 1(c)] can be better fitted by the elastic force by taking into account the anchoring energy (Fig. S6(a) [41]).

D. Stick-slip regime

Similarly, the critical anchoring torque $\Gamma_c \approx 0.0148$ mN/m, the anchoring strength $W \approx 0.0073$ mN/m, and $\frac{\Phi_0 - \Phi}{2} \approx 116.4^\circ$ for the second regime were calculated from the slope and intersection in Fig. 3(b). These values were used to predict the positions where consecutive jumps occur, as shown in Fig. 3(c). The critical jumping distances fit the experimental data very well. However, the measured forces [Fig. 1(d)] are worse fitted by the elastic theory considering the anchoring energy [Fig. S6(b) [41]]. It is as if the surface torque is correct but the composition of the torque is not a pure anchoring torque. Possibly, the surface viscosity may start to become important in this regime with medium anchoring strength. Alternatively, the two-thirds coverage of mica on the lenses may cause slip on this regime after water adsorption, since the premier critical compression ratio [Fig. 1(d)] is similar to the compression ratio where K_{22} changes from a larger value to 3.8 pN in the first regime, as shown in Fig. 1(c). Last but not least, the surface torque may be balanced by the viscoelastic torque in the stick-slip regime.

In the second regime, no defects are observed stretching on the surface during either approach or retraction, indicating that the defects are in the bisector of surfaces and the polar anchoring strength [55] is larger than $2\sqrt{\frac{3}{8}K_{33}B} \approx 0.4$ mN/m, where $K_{33} = 27.5$ pN is the bend elastic constant, and B is the dilation term. It seems reasonable that the azimuthal anchoring strength is one or two orders of magnitude smaller than

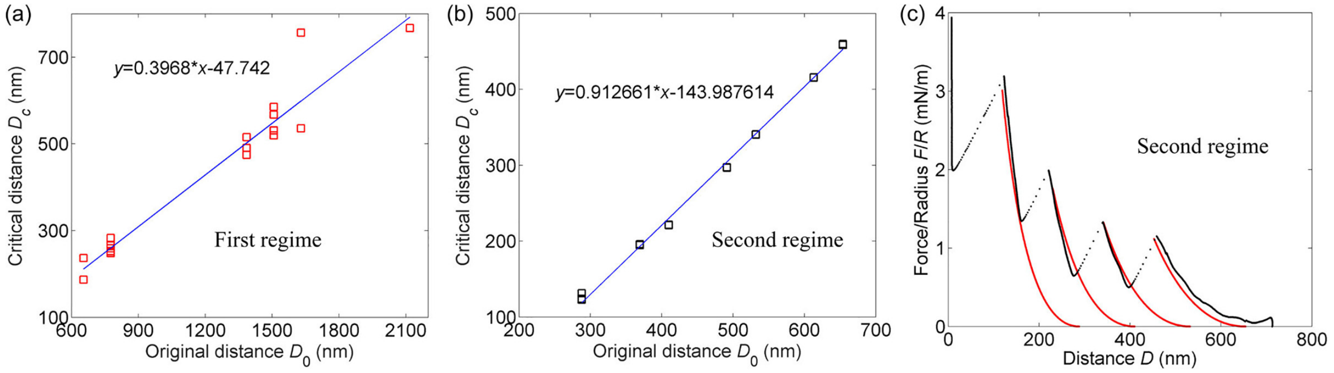

FIG. 3. Calculation of the anchoring strength. The critical jumping distance D_c as a function of the original distance D_0 in (a) the first regime and (b) the second regime (including all the stick-slip jumps); the blue line is the linear trend line. (c) Fitting the force profile (black, upper) in the second regime by Eqs. (4) and (10) with $K_{22} = 6$ pN and the critical surface torque and anchoring strength obtained from (b).

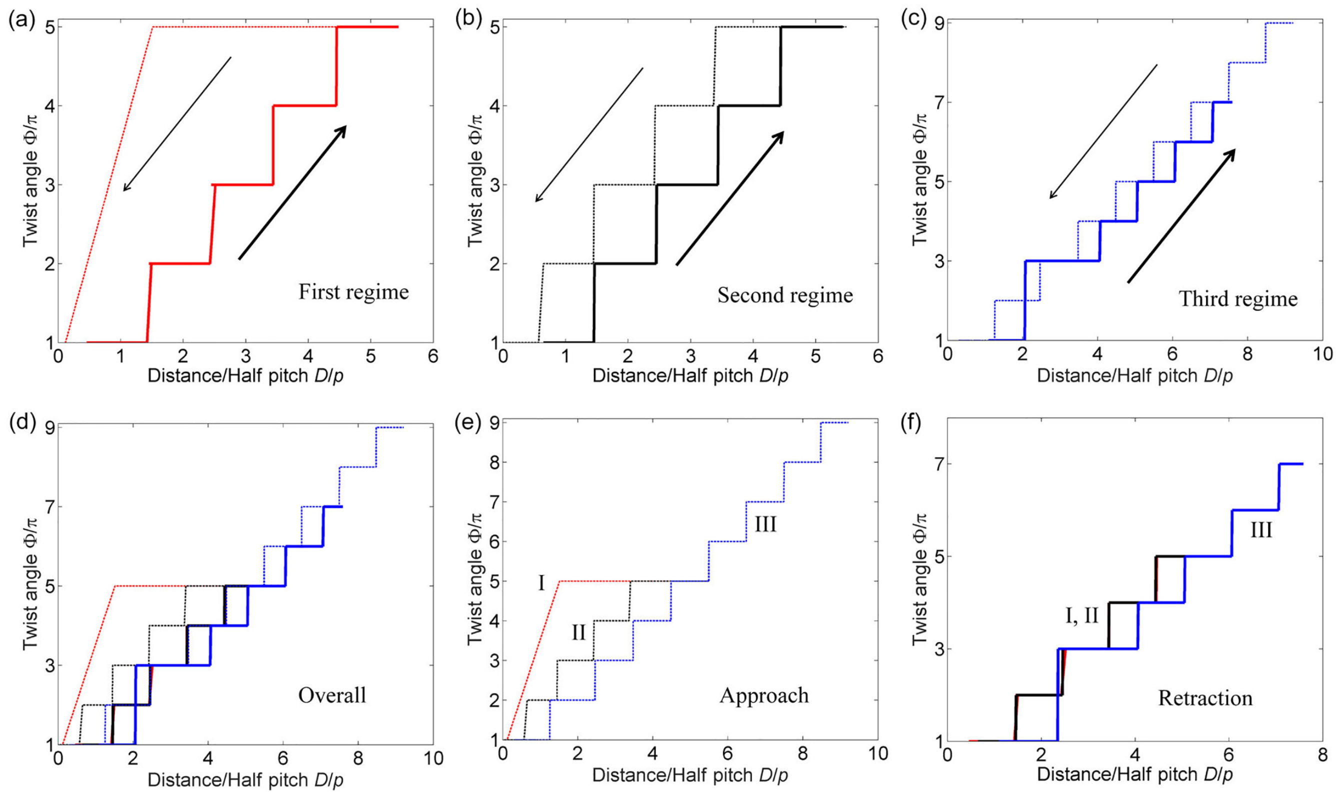

FIG. 4. Hysteresis of the twist angle in three regimes. The noninteger layer has been deducted to eliminate the difference of easy axes among different experiments. (a) First regime. The twist angle during the jump process is assumed to keep a constant compression ratio but decrease the total twist angle. (b) Second regime. (c) Third regime. The deviation of the anchoring angle is ignored in all three regimes. (d) Three regimes. (e) Approach profiles of I–III three regimes. (f) Retraction profiles of I–III three regimes. Thin and thick lines following the direction of the arrow are approach and retraction profiles, respectively. The red, black, and blue lines denote the three regimes, respectively.

the polar anchoring [66]. Then the polar anchoring strength in the first regime would be very large.

E. Sliding-slip regime

For weak anchoring, the anchoring torque is negligible [29]. Therefore, the elastic torque is mainly balanced by the surface viscosity. As a result, the surface viscosity can be estimated as $\gamma_s = 1.83 \times 10^{-4}$ Pa s m, and the corresponding viscous force is about 0.8 mN/s at a distance $D_0 = 1000$ nm (see Sec. SIV of the Supplemental Material [41]), which is very close to the background force in the third regime [Fig. 1(b)]. This background force may be related to the commonly observed background forces with liquid crystals in the SFB [48,61] (see Sec. SIV of the Supplemental Material [41]).

In fact, the discontinuous twist transition has been attributed to surface anchoring by most past studies [7,12–29,31–35], among which only some [20,28,29,32] used the concept of surface torque to explain the mechanism. However, many of them [14,16–18,22–26,33,35] differentiated the anchoring energy G with respect to the twist angle $\partial G/\partial \Phi$, which is actually the form of torque. The surface torque has long been adopted to describe the surface forces imposed on liquid crystals [5,67–72], but this concept does not seem to be widely used in the liquid crystal community. In a recent study [37] explaining the discontinuous transition with the energy barrier from dislocation defects, the integrating range of the equations for calculating the nucleation energy should not be the same for different layers (see Sec. SII of the Supplemental Material [41]). Therefore, the conclusions about the energy barrier may require reassessment.

F. Hysteresis

Figure 4 shows that hysteresis of the twist angle between retraction and approach exists in all three regimes and decreases with time evolution. The twist angles can be further confirmed by the 4×4 matrix simulation [40,62] (Fig. S7 [41]). In particular, multiple-layer jumping events occur during both approach and retraction [Figs. 4(a) and 4(c)]. Figure 4(f) shows that the retraction profiles are the same in the first two regimes and a delayed jump resulting from the viscous stretch on the surface (see Movie S1 and Sec. SIV of the Supplemental Material [41]) is observed in the third regime. Notably, the twist angle profile during the approach in the third regime is coincident with the profile during retraction in the first two regimes, as shown in Fig. 4(d), indicating negligible anchoring torque during the approach. Most of the jumping points occur at integer quarter pitch distances, but more uncertainties are observed at small distances.

The noninteger layers were deduced in three regimes, assuming no change in the direction of the easy axis. Indeed, the twist angle profiles in the first and second regimes overlay with each other during retraction [Fig. 4(f)], confirming the same anchoring direction. Regarding the third regime, retraction profiles cannot be compared with the others because of the viscous stretch on the surface. However, the simulation in Fig. S7 [41] did not consider the anchoring transition but can still fit the data very well, indicating no change of the easy axis. The possible first-order anchoring transition on mica [38] is either 60° or 90°, which can be easily detected by the simulation [40,62]. During approach, the forced anchoring transition may accompany stress-induced anchoring deviation and viscous stretch, resulting in jumps. This situation is more complicated and no clear evidence was observed in this work. Furthermore, the simulation is not sensitive enough to distinguish anchoring deviation in highly compressed layers [62]. Overall, the anchoring transition may require more investigation.

During retraction and approach, the mechanical responses are very different, showing hysteresis, which can be understood by analogy to fracture in solid materials during tension and compression. However, given the complexity of the analogy from solids to liquid crystals, this topic will be discussed in a separate paper.

IV. CONCLUSION

In conclusion, three regimes were observed in cholesterics during mechanical compression in the SFB. The elastic torque of cholesterics is balanced by the surface torque, which consists of anchoring torque and viscous torque. In the constrained regime with strong anchoring, the anchoring torque dominates, while the viscous torque dominates in the sliding-slip regime with weak anchoring. In the stick-slip regime, both anchoring torque and viscous torque as well as mica coverage are possible to affect the stick-slip. This study provides a method based on the critical surface torque to measure strong anchoring strength and deviation. The surface torque, i.e., frictional torque in rotational friction, elucidates the dynamics of static friction [73,74], as evidenced by the deviation of the anchoring angle and the hysteresis of the twist angle. This study sheds light on the understanding of boundary effects on permeative flows [75,76], friction [77], yield stress materials [3,78], adhesions, and biomechanics.

V. METHODS

A. Materials

The nematics (QYPDLC-036, similar to BL036 from Merck) and the chiral dopant (R2011, right-handed) were purchased from Qingdao QY Liquid Crystal Co., Ltd. (Chengyang, Qingdao, China). Cholesterics were mixed with 62.4 wt % nematics and 37.6 wt % chiral dopants, resulting in a pitch length of about 244 nm. The small pitch well fits the typical measuring range of 0–1000 nm in the SFB.

B. Sample preparation

Cholesterics were dried in a Schlenk line (60 °C) overnight before the experiments. The muscovite mica surfaces with a thickness of 3.3 μm were glued onto cylinders (radius of 1 cm) in the SFB. The chamber of the SFB was purged with dry nitrogen for 1 h before injecting the sample. Some phosphorus pentoxide was left in the chamber as the desiccant. The experiments lasted for several days to obtain decayed anchoring strength.

When cholesterics were put on a freshly cleaved mica surface, a strong planar anchoring was obtained. The liquid crystal molecules on the surface pointed toward a single direction, called the easy axis. As mica is a natural crystal [5], the strong planar anchoring status was assured and confirmed by our previous cholesteric study [40] and the other study with nematics [38]. By increasing the humidity, the anchoring direction on mica may change by 60° or 90° within the azimuthal plane [38], but a clear transition was not observed in this work.

ACKNOWLEDGMENTS

W.Z. is very grateful to S. Perkin for her generous help and insightful guidance on the project. S.P. suggested using the torque balance to analyze the data and the harmonic elastic potential to demonstrate the second regime. S.P. also contributed to the design of the experiments and the analysis of several figures. W.Z. thanks R. Lhermerout for his derivation of equations calculating the anchoring strength, critical torque, and anchoring deviation. W.Z. is very grateful to C.S. Perez-Martinez for her assistance with some experiments. W.Z. acknowledges J. Hallett and B. Zappone for helpful discussions. This work was supported by the European Research Council (Grant No. ERC-2015-StG-676861) and the European Union's Horizon 2020 research and innovation programme under Grant No. 674979-NANOTRANS.

---

[1] A. J. Grass, Structural features of turbulent flow over smooth and rough boundaries, J. Fluid Mech. **50**, 233 (1971).

[2] E. Lauga, M. Brenner, and H. Stone, Microfluidics: The no-slip boundary condition, in *Springer Handbook of Experimental Fluid Mechanics*, edited by C. Tropea, A. L. Yarin, and J. F. Foss (Springer, Berlin, 2007), p. 1219.

[3] D. Bonn, M. M. Denn, L. Berthier, T. Divoux, and S. Manneville, Yield stress materials in soft condensed matter, Rev. Mod. Phys. **89**, 035005 (2017).

[4] P. Sheng, Boundary-layer phase-transition in nematic liquid-crystals, Phys. Rev. A **26**, 1610 (1982).

[5] P.-G. De Gennes and J. Prost, *The Physics of Liquid Crystals*, 2nd ed. (Clarendon Press, Oxford, 1993).

[6] V. Fréedericksz and V. Zolina, Forces causing the orientation of an anisotropic liquid, Trans. Faraday Soc. **29**, 919 (1933).

[7] R. B. Meyer, Effects of electric and magnetic fields on structure of cholesteric liquid crystals, Appl. Phys. Lett. **12**, 281 (1968).

[8] H. Baessler and M. M. Labes, Relationship between electric field strength and helix pitch in induced cholesteric-nematic phase transitions, Phys. Rev. Lett. **21**, 1791 (1968).

[9] R. B. Meyer, Distortion of a cholesteric structure by a magnetic field, Appl. Phys. Lett. **14**, 208 (1969).

[10] G. Durand, L. Leger, F. Rondelez, and M. Veyssie, Magnetically induced cholesteric-to-nematic phase transition in liquid crystals, Phys. Rev. Lett. **22**, 227 (1969).

[11] F. J. Kahn, Electric-field-induced color changes and pitch dilation in cholesteric liquid crystals, Phys. Rev. Lett. **24**, 209 (1970).

[12] S. V. Belyaev and L. M. Blinov, Step unwinding of a spiral in a cholesteric liquid crystal, JETP Lett. **30**, 99 (1979).

[13] R. Dreher, Remarks on distortion of a cholesteric structure by a magnetic-field, Solid State Commun. **13**, 1571 (1973).

[14] I. P. Pinkevich, V. Y. Reshetnyak, Y. A. Reznikov, and L. G. Grechko, Influence of light-induced molecular conformational transformations and anchoring energy on cholesteric liquid-crystal pitch and dielectric-properties, Mol. Cryst. Liq. Cryst. **222**, 269 (1992).

[15] P. J. Kedney and I. W. Stewart, The untwisting of a bounded sample of cholesteric liquid crystal, Continuum Mech. Thermodyn. **6**, 141 (1994).

[16] H. Zink and V. A. Belyakov, Determination of changes in director orientation with temperature in oriented cholesteric layers, Mol. Cryst. Liq. Cryst. **282**, 17 (1996).

[17] M. Warner, E. M. Terentjev, R. B. Meyer, and Y. Mao, Untwisting of a cholesteric elastomer by a mechanical field, Phys. Rev. Lett. **85**, 2320 (2000).

[18] S. P. Palto, On mechanisms of the helix pitch variation in a thin cholesteric layer confined between two surfaces, J. Exp. Theor. Phys. **94**, 260 (2002).

[19] H. Q. Xianyu, S. Faris, and G. P. Crawford, In-plane switching of cholesteric liquid crystals for visible and near-infrared applications, Appl. Opt. **43**, 5006 (2004).

[20] V. A. Belyakov, I. W. Stewart, and M. A. Osipov, Surface anchoring and dynamics of jump-wise director reorientations in planar cholesteric layers, Phys. Rev. E **71**, 051708 (2005).

[21] S. Uto, A helix unwinding process in ferroelectric liquid crystals with fixed boundaries, J. Appl. Phys. **97**, 014107 (2005).

[22] A. D. Kiselev and T. J. Sluckin, Twist of cholesteric liquid crystal cells: Stability of helical structures and anchoring energy effects, Phys. Rev. E **71**, 031704 (2005).

[23] G. Mckay, Bistable surface anchoring and hysteresis of pitch jumps in a planar cholesteric liquid crystal, Eur. Phys. J. E **35**, 1 (2012).

[24] I. Lelidis, G. Barbero, and A. L. Alexe-Ionescu, Cholesteric pitch transitions induced by mechanical strain, Phys. Rev. E **87**, 022503 (2013).

[25] A. N. Zakhlevnykh and V. S. Shavkunov, Magnetic-field-induced stepwise director reorientation and untwisting of a planar cholesteric structure with finite anchoring energy, Phys. Rev. E **94**, 042708 (2016).

[26] G. Barbero, W. Zheng, and B. Zappone, Twist transitions and force generation in cholesteric liquid crystal films, J. Mol. Liq. **267**, 242 (2018).

[27] S. S. Tenishchev, A. D. Kiselev, A. V. Ivanov, and V. M. Uzdin, Multiple minimum-energy paths and scenarios of unwinding transitions in chiral nematic liquid crystals, Phys. Rev. E **100**, 062704 (2019).

[28] R. F. de Souza, E. K. Lenzi, R. T. de Souza, L. R. Evangelista, Q. Li, and R. S. Zola, Surface induced twist in nematic and chiral nematic liquid crystals: Stick-slip-like and constrained motion, Soft Matter **14**, 2084 (2018).

[29] P. Oswald, A. Dequidt, and A. Zywocinski, Sliding planar anchoring and viscous surface torque in a cholesteric liquid crystal, Phys. Rev. E **77**, 061703 (2008).

[30] R. F. de Souza, D. K. Yang, E. K. Lenzi, L. R. Evangelista, and R. S. Zola, Effect of surface viscosity, anchoring energy, and cell gap on the response time of nematic liquid crystals, Ann. Phys. **346**, 14 (2014).

[31] K. Funamoto, M. Ozaki, and K. Yoshino, Discontinuous shift of lasing wavelength with temperature in cholesteric liquid crystal, Jpn. J. Appl. Phys. **42**, L1523 (2003).

[32] M. F. Moreira, I. C. S. Carvalho, W. Cao, C. Bailey, B. Taheri, and P. Palffy-Muhoray, Cholesteric liquid-crystal laser as an optic fiber-based temperature sensor, Appl. Phys. Lett. **85**, 2691 (2004).

[33] H. G. Yoon, N. W. Roberts, and H. F. Gleeson, An experimental investigation of discrete changes in pitch in a thin, planar chiral nematic device, Liq. Cryst. **33**, 503 (2006).

[34] M. Skarabot, Z. Lokar, K. Gabrijelcic, D. Wilkes, and I. Musevic, Atomic force microscope based method of measuring short cholesteric pitch in liquid crystals, Liq. Cryst. **38**, 1017 (2011).

[35] T. N. Orlova, R. I. Iegorov, and A. D. Kiselev, Light-induced pitch transitions in photosensitive cholesteric liquid crystals: Effects of anchoring energy, Phys. Rev. E **89**, 012503 (2014).

[36] S. P. Palto, M. I. Barnik, A. R. Geivandov, I. V. Kasyanova, and V. S. Palto, Spectral and polarization structure of field-induced photonic bands in cholesteric liquid crystals, Phys. Rev. E **92**, 032502 (2015).

[37] B. Zappone and R. Bartolino, Topological barriers to defect nucleation generate large mechanical forces in an ordered fluid, Proc. Natl. Acad. Sci. USA **118**, e211050311 (2021).

[38] P. Pieranski and B. Jérôme, Adsorption-induced anchoring transitions at nematic-liquid-crystal-crystal interfaces, Phys. Rev. A **40**, 317 (1989).

[39] B. Jerome and Y. R. Shen, Anchoring of nematic liquid crystals on mica in the presence of volatile molecules, Phys. Rev. E **48**, 4556 (1993).

[40] W. C. Zheng, C. S. Perez-Martinez, G. Petriashvili, S. Perkin, and B. Zappone, Direct measurements of structural forces and twist transitions in cholesteric liquid crystal films with a surface force apparatus, Soft Matter **15**, 4905 (2019).

[41] See Supplemental Material at http://link.aps.org/supplemental/10.1103/PhysRevE.109.044701 for experimental details, defect energy, and simulations.

[42] P. Richetti, P. Kekicheff, J. L. Parker, and B. W. Ninham, Measurement of the interactions between membranes in a stack, Nature (London) **346**, 252 (1990).

[43] J. Klein, Forces between mica surfaces bearing adsorbed macromolecules in liquid-media, J. Chem. Soc., Faraday Trans. I **79**, 99 (1983).

[44] J. Klein and E. Kumacheva, Simple liquids confined to molecularly thin layers. I. Confinement-induced liquid-to-solid phase transitions, J. Chem. Phys. **108**, 6996 (1998).

[45] J. N. Israelachvili, Thin film studies using multiple-beam interferometry, J. Colloid Interface Sci. **44**, 259 (1973).

[46] J. Israelachvili *et al.*, Recent advances in the surface forces apparatus (SFA) technique, Rep. Prog. Phys. **73**, 036601 (2010).

[47] M. J. Park and O. O. Park, Alignment of liquid crystals on a topographically nano-patterned polymer surface prepared by a soft-imprint technique, Microelectron. Eng. **85**, 2261 (2008).

[48] R. G. Horn, J. N. Israelachvili, and E. Perez, Forces due to structure in a thin liquid crystal film, J. Phys. **42**, 39 (1981).

[49] P. Richetti, P. Kékicheff, and P. Barois, Measurement of the layer compressibility modulus of a lamellar mesophase with a surface forces apparatus, J. Phys. II **5**, 1129 (1995).

[50] I. I. Smalyukh and O. D. Lavrentovich, Three-dimensional director structures of defects in Grandjean-Cano wedges of cholesteric liquid crystals studied by fluorescence confocal polarizing microscopy, Phys. Rev. E **66**, 051703 (2002).

[51] O. D. Lavrentovich and D. K. Yang, Cholesteric cellular patterns with electric-field-controlled line tension, Phys. Rev. E **57**, R6269 (1998).

[52] I. I. Smalyukh, B. I. Senyuk, S. V. Shiyanovskii, O. D. Lavrentovich, A. N. Kuzmin, A. V. Kachynski, and P. N. Prasad, Optical trapping, manipulation, and 3D imaging of disclinations in liquid crystals and measurement of their line tension, Mol. Cryst. Liq. Cryst. **450**, 279 (2006).

[53] P. Pieranski, Cholesteric dislocations in mica wedges, Liq. Cryst. Rev. **10**, 6 (2022).

[54] M. Zapotocky, L. Ramos, P. Poulin, T. C. Lubensky, and D. A. Weitz, Particle-stabilized defect gel in cholesteric liquid crystals, Science **283**, 209 (1999).

[55] I. I. Smalyukh and O. D. Lavrentovich, Anchoring-mediated interaction of edge dislocations with bounding surfaces in confined cholesteric liquid crystals, Phys. Rev. Lett. **90**, 085503 (2003).

[56] R. A. Herke, N. A. Clark, and M. A. Handschy, Stress-induced vortex line helixing avalanches in the plastic-flow of a smectic A liquid-crystal, Science **267**, 651 (1995).

[57] R. A. Herke, N. A. Clark, and M. A. Handschy, Dynamic behavior of oscillatory plastic flow in a smectic liquid crystal, Phys. Rev. E **56**, 3028 (1997).

[58] C. Blanc, N. Zuodar, I. Lelidis, M. Kleman, and J. L. Martin, Defect dynamics in a smectic Grandjean-Cano wedge, Phys. Rev. E **69**, 011705 (2004).

[59] C. Blanc, N. Zuodar, J. L. Martin, I. Lelidis, and M. Kleman, Role of microscopic defects in the plasticity of lamellar materials, Mol. Cryst. Liq. Cryst. **412**, 85 (2004).

[60] I. Lelidis, C. Blanc, and M. Kleman, Optical and confocal microscopy observations of screw dislocations in smectic-*A* liquid crystals, Phys. Rev. E **74**, 051710 (2006).

[61] M. Ruths, S. Steinberg, and J. N. Israelachvili, Effects of confinement and shear on the properties of thin films of thermotropic liquid crystal, Langmuir **12**, 6637 (1996).

[62] B. Zappone, W. C. Zheng, and S. Perkin, Multiple-beam optical interferometry of anisotropic soft materials nanoconfined with the surface force apparatus, Rev. Sci. Instrum. **89**, 085112 (2018).

[63] P. A. Thompson and M. O. Robbins, Shear-flow near solids: Epitaxial order and flow boundary-conditions, Phys. Rev. A **41**, 6830 (1990).

[64] Rotational friction, https://uk.mathworks.com/help/physmod/simscape/ref/rotationalfriction.html.

[65] D. V. Shmeliova and V. A. Belyakov, Director distribution in Grandjean-Cano wedge and restoration of surface anchoring potential, Mol. Cryst. Liq. Cryst. **646**, 160 (2017).

[66] B. Jerome, Surface effects and anchoring in liquid crystals, Rep. Prog. Phys. **54**, 391 (1991).

[67] J. L. Ericksen, Conservation laws for liquid crystals, Trans. Soc. Rheol. **5**, 23 (1961).

[68] J. L. Ericksen, Hydrostatic theory of liquid crystals, Arch. Ration. Mech. Anal. **9**, 371 (1962).

[69] J. Basterfield, W. Miller, and G. Weatherly, Anisotropy of interfacial free energy in solid-fluid and solid-solid systems, Can. Metall. Q. **8**, 131 (1969).

[70] M. J. Stephen and J. P. Straley, Physics of liquid crystals, Rev. Mod. Phys. **46**, 617 (1974).

[71] S. Chandrasekhar, *Liquid Crystals*, Cambridge Monographs on Physics (Cambridge University Press, Cambridge, 1977).

[72] P. C. Martin, O. Parodi, and P. S. Pershan, Unified hydrodynamic theory for crystals, liquid-crystals, and normal fluids, Phys. Rev. A **6**, 2401 (1972).

[73] M. H. Muser, How static is static friction? Proc. Natl. Acad. Sci. USA **105**, 13187 (2008).

[74] Z. P. Yang, H. P. Zhang, and M. Marder, Dynamics of static friction between steel and silicon, Proc. Natl. Acad. Sci. USA **105**, 13264 (2008).

[75] D. Marenduzzo, E. Orlandini, and J. M. Yeomans, Permeative flows in cholesteric liquid crystals, Phys. Rev. Lett. **92**, 188301 (2004).

[76] W. Helfrich, Capillary flow of cholesteric and smectic liquid crystals, Phys. Rev. Lett. **23**, 372 (1969).

[77] T. G. Sano, T. Yamaguchi, and H. Wada, Slip morphology of elastic strips on frictional rigid substrates, Phys. Rev. Lett. **118**, 178001 (2017).

[78] P. C. F. Moller, A. Fall, and D. Bonn, Origin of apparent viscosity in yield stress fluids below yielding, Europhys. Lett. **87**, 38004 (2009).